Constraining neutrino oscillation parameters with current solar and atmospheric data

M. Maltoni,[1,*] T. Schwetz,[2,†] M. A. Tórtola,[1,‡] and J. W. F. Valle[1,§]
[1]*Instituto de Física Corpuscular – C.S.I.C./Universitat de València, Edificio Institutos de Paterna, Apt 22085, E–46071 Valencia, Spain*
[2]*Institut für Theoretische Physik, Universität Wien, Boltzmanngasse 5, A–1090 Wien, Austria*
(Received 22 July 2002; published 30 January 2003)

We analyze the impact of recent solar and atmospheric data on the determination of the neutrino oscillation parameters, taking into account that both the solar ν_e and the atmospheric ν_μ may convert to a mixture of active and sterile neutrinos. We use the most recent global solar neutrino data, including the 1496-day Super-K neutrino data sample, and we investigate in detail the impact of the recent Sudbury Neutrino Observatory (SNO) neutral current, spectral, and day/night data by performing also an analysis using only the charged current rate from SNO. We confirm the clear preference of the pure active large mixing angle solution of the solar neutrino problem and obtain that the LOW solution, vacuum oscillation, small mixing angle, and just-so^2 solutions are disfavored with a $\Delta\chi^2 = 9,\ 9,\ 23,\ 31$, respectively. Furthermore, we find that the global solar data constrains the admixture of a sterile neutrino to be less than 44% at 99% C.L. A pure sterile solution is ruled out with respect to the active one at 99.997% C.L. By performing an improved fit of the atmospheric data, we also update the corresponding regions of oscillation parameters. We find that the recent atmospheric Super-K (1489-day) and MACRO data have a strong impact on constraining a sterile component in atmospheric oscillations: if the ν_μ is restricted to the atmospheric mass states only a sterile admixture of 16% is allowed at 99% C.L., while a bound of 35% is obtained in the unconstrained case. Pure sterile oscillations are disfavored with a $\Delta\chi^2 = 34.6$ compared to the pure active case.

DOI: 10.1103/PhysRevD.67.013011 PACS number(s): 14.60.Pq, 14.60.Lm, 14.60.St, 26.65.+t

I. INTRODUCTION

Apart from confirming, yet again, the long-standing solar neutrino problem [1–5], the recent results from the Sudbury Neutrino Observatory (SNO) on neutral current (NC) events [6,7] have given strong evidence that solar neutrinos convert mainly to an active neutrino flavor. In addition, valuable spectral and day/night information has been provided [6,7]. This adds to the already robust evidence that an extension of the standard model of particle physics is necessary in the lepton sector. Although certainly not yet unique, at least for the case of solar neutrinos, which can be accounted for well by spin-flavor precession [8,9] or nonstandard neutrino matter interactions [10], the most popular joint explanation of solar and atmospheric experiments is provided by the neutrino oscillations hypothesis, with neutrino mass-squared differences of the order of $\Delta m^2_{\rm SOL} \lesssim 10^{-4}$ eV^2 and $\Delta m^2_{\rm ATM} \sim 3 \times 10^{-3}$ eV^2, respectively.

In the wake of the recent SNO NC results we have reanalyzed the global status of current neutrino oscillation data including these and the remaining solar data [1–7] as well as the current atmospheric [11,12] samples, including the 1489 day Super-Kamiokande data [13] and the most recent MACRO data [14]. Motivated by the stringent limits from reactor experiments [15] we adopt an effective two-neutrino approach in which solar and atmospheric analyses decouple. However, our effective two-neutrino approach is generalized in the sense that it takes into account that a light sterile neutrino [16–21], advocated to account for the Liquid Scintillation Neutrino Detector (LSND) anomaly [22], may take part in both solar and atmospheric conversions. The natural setting for such a light sterile neutrino is provided by four-neutrino models. In this paper we will determine the constraints on oscillation parameters in this generalized scenario following from solar and atmospheric data separately. Such separate analyses are necessary ingredients towards a combined analysis of all current oscillation data, including solar, atmospheric, negative short-baseline data and the LSND experiment [23,24]. As shown in Ref. [23] such separate analyses can be performed independently of the details of the four-neutrino mass scheme.

Since the release of the latest SNO data in April 2002 a number of global solar neutrino analyses in terms of active oscillations have appeared [9,25–31]. Moreover, it has been shown by model-independent comparisons of the SNO charged current (CC) rate with the SNO NC and Super-K rates that transitions of solar neutrinos into sterile neutrinos are strongly constrained by the recent data (see, e.g., Refs. [6,26–28]). However, so far no dedicated global analyses exist where a participation of a sterile neutrino in the oscillations is fully taken into account.[1] Here we present a complete solar neutrino analysis including sterile neutrinos, determining the allowed ranges for the oscillation parameters $\theta_{\rm SOL}$ and $\Delta m^2_{\rm SOL}$, as well as for the parameter $0 \leqslant \eta_s \leqslant 1$

*Electronic address: maltoni@ific.uv.es
†Electronic address: schwetz@thp.univie.ac.at
‡Electronic address: mariam@ific.uv.es
§Electronic address: valle@ific.uv.es

[1]In Ref. [32] admixtures of a sterile neutrino to solar oscillations are considered. However, the authors of Ref. [32] are mainly interested in the determination of the solar neutrino fluxes and hence their results are complementary to those obtained here. Some considerations of sterile solar neutrino oscillations can also be found in Ref. [30].

 ©2003 The American Physical Society

describing the active-sterile admixture. Furthermore, we investigate in detail the impact of the SNO neutral current, spectral, and day/night data and compare with an analysis where we use only the charged current rate from SNO.

Concerning the atmospheric data, we perform an update of previous analyses [23,33], adopting again the most general parametrization of atmospheric neutrino oscillations in the presence of sterile neutrino mixing, characterized by four parameters. We find that the recent 1489-day Super-Kamiokande data combined with the latest MACRO data lead to considerably stronger rejection against a sterile neutrino contribution to the oscillations than the previous 1289-day data sample.

The plan of the paper is as follows. In Sec. II A we set the general parametrization for solar oscillations in the presence of active-sterile mixing. In Sec. II B we briefly describe the solar neutrino data and their analysis. In Sec. II C we present the results of our analysis, aimed at studying the impact of recent solar data in the determination of the solar neutrino oscillation parameters, assuming, as mentioned, that the ν_e may convert to a mixture of active and sterile neutrinos. We give the regions of oscillation parameters for different allowed η_s values, display the global behavior of $\Delta\chi^2_{\rm SOL}(\Delta m^2_{\rm SOL})$ and $\Delta\chi^2_{\rm SOL}(\theta_{\rm SOL})$, calculated with respect to the favored active large mixing angle (LMA) solution, and evaluate the impact of the SNO NC, spectral, and day/night data. Present solar data exhibit a higher degree of rejection against non-LMA and/or nonactive oscillation solutions, which we quantify, giving also the absolute goodness of fit (GOF) of various oscillation solutions. Our solar neutrino results are briefly compared with those obtained in other recent analyses in Sec. II D. In Sec. III A we set our notations for atmospheric oscillations in the presence of active-sterile admixture. In Sec. III B we briefly describe the atmospheric neutrino data and their analysis. In Sec. III C we describe our results for atmospheric oscillation parameters in an improved global fit of current atmospheric neutrino data. We quantify the impact both of our improved analysis as well as that of the recent data in rejecting against the sterile oscillation hypothesis. We update the corresponding regions of oscillation parameters and display the global behavior of $\Delta\chi^2_{\rm ATM}(\Delta m^2_{\rm ATM})$ and $\Delta\chi^2_{\rm ATM}(\theta_{\rm ATM})$. We compare the situation before and after the recent 1489-day atmospheric Super-K data samples and give the present GOF of the oscillation hypothesis. In Sec. III D, we briefly compare our atmospheric neutrino results with those of other analyses. Finally, in Sec. IV we present our conclusions.

II. SOLAR NEUTRINOS

A. Active-sterile solar neutrino oscillations

In the following we will analyze solar neutrino data in the general framework of mixed active-sterile neutrino oscillations. In this case the electron neutrino produced in the sun converts into a combination of an active nonelectron neutrino ν_x (which again is a combination of ν_μ and ν_τ) and a sterile neutrino ν_s:

$$\nu_e \to \sqrt{1-\eta_s}\ \ \nu_x + \sqrt{\eta_s}\ \ \nu_s\,. \tag{1}$$

The parameter η_s with $0 \leqslant \eta_s \leqslant 1$ describes the fraction of the sterile neutrino participating in the solar oscillations. Therefore the oscillation probabilities depend on the three parameters $\Delta m^2_{\rm SOL}$, $\theta_{\rm SOL}$, and η_s. The natural framework of light sterile neutrinos participating in oscillations are four-neutrino mass schemes, proposed to account for the LSND result [22] in addition to solar and atmospheric neutrino oscillations. For previous studies of solar neutrino oscillation in a four-neutrino framework see Refs. [21,33,34] and for an exact definition of the solar parameters and adopted approximations see Ref. [23].

B. Data and analysis

As experimental data, we use the solar neutrino rates of the chlorine experiment Homestake [2] ($2.56 \pm 0.16 \pm 0.16$ SNU), the most recent result of the gallium experiments SAGE [3] ($70.8\ ^{+5.3}_{-5.2}\ ^{+3.7}_{-3.2}$ SNU) and GALLEX/GNO [4] ($70.8 \pm 4.5 \pm 3.8$ SNU), as well as the 1496-days Super-Kamiokande data sample [1] in the form of 44 bins (eight energy bins, six of which are further divided into seven zenith angle bins). In addition to this, we include the latest results from SNO presented in Refs. [6,7], in the form of 34 data bins (17 energy bins for each day and night period). Therefore in our statistical analysis we use $3+44+34=81$ observables, which we fit in terms of the three parameters $\Delta m^2_{\rm SOL}$, $\theta_{\rm SOL}$, and η_s, with a $\chi^2_{\rm SOL}$ of the form

$$\chi^2_{\rm SOL}(\Delta m^2_{\rm SOL}, \theta_{\rm SOL}, \eta_s) = \sum_{i,j=1}^{81} (R_i^{ex} - R_i^{th}) \cdot (\sigma^2_{ex} + \sigma^2_{th})^{-1}_{ij} \cdot (R_j^{ex} - R_j^{th}). \tag{2}$$

In order to fully isolate the impact of the recent neutral current, spectral, and day/night information of the SNO result, we also present an analysis which does not include such information. To this aim we use only the SNO events with energy higher than 6.75 MeV, for which the NC component is negligible [5]. We sum these events to a single rate, combining with Cl, Ga rates and full Super-K data, as described above. This procedure is analogous to the pre-SNO-NC situation, except that we take advantage of the enhanced statistics on the CC rate provided by the new data. We will refer to this analysis as $\mathrm{SNO}^{\rm rate}_{\rm CC}$ analysis and it contains 48 data points. The comparison with the analysis including the complete SNO data published this year ($\mathrm{SNO}^{\rm SP,DN}_{\rm CC,NC}$) allows us to highlight the impact of the SNO NC, spectral, and day/night information.

For the solar neutrino fluxes we use the standard solar model (SSM) flux [35], including its standard ^{8}B flux prediction.[2] Motivated by the excellent agreement of the recent SNO NC result with the predictions of the standard solar model, we prefer to adopt a boron-fixed analysis. However, for the case of the LMA solution we explicitly illustrate

[2]We choose not to include the flux indicated by the recent S_{17} measurement of Ref. [36].

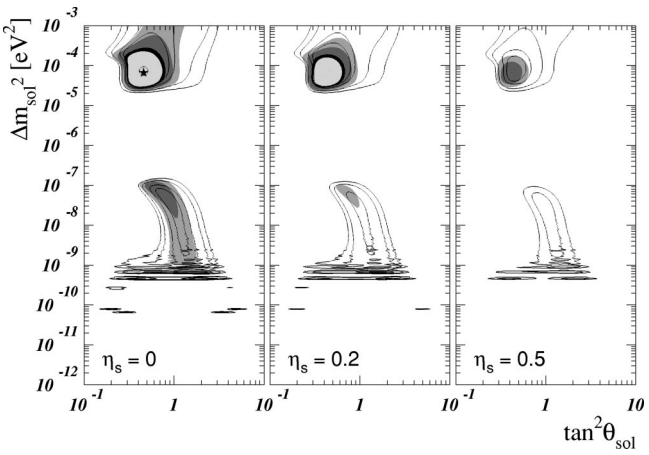

FIG. 1. Allowed regions of $\tan^2\theta_{\rm SOL}$ and $\Delta m^2_{\rm SOL}$ for $\eta_s=0$ (active oscillations), $\eta_s=0.2$, and $\eta_s=0.5$. The lines indicate the regions determined by the $\rm SNO^{rate}_{CC}$ analysis (see definition in text), the shaded regions correspond to $\rm SNO^{SP,DN}_{CC,NC}$ (see text). The confidence levels are 90%, 95%, 99%, and 3σ for 3 degrees of freedom.

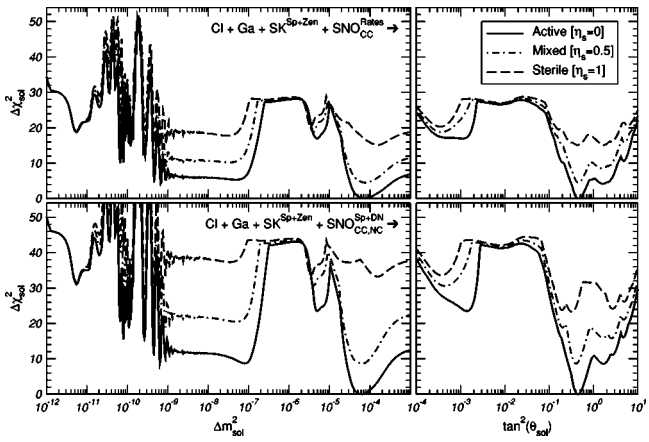

FIG. 2. $\Delta\chi^2_{\rm SOL}$ as a function of $\Delta m^2_{\rm SOL}$ and $\tan^2\theta_{\rm SOL}$, for pure active ($\eta_s=0$), pure sterile ($\eta_s=1$), and mixed neutrino oscillations ($\eta_s=0.5$). Upper and lower panels correspond to the $\rm SNO^{rate}_{CC}$ and $\rm SNO^{SP,DN}_{CC,NC}$ samples defined in text.

the effect of this assumption by performing also a boron-free analysis, where we treat the solar ^{8}B flux as free parameter in the fit. For simplicity we neglect the *hep* and *F* neutrino fluxes, whose contribution to the present solar neutrino experiments is marginal, while for the *pp*, Be, B, *pep*, N, and O fluxes we use the SSM value given in Ref. [35], taking properly into account their theoretical uncertainties and cross correlations in the calculation of the χ^2 function.

For the neutrino cross sections of chlorine, SAGE, GALLEX/GNO, and Super-K we assume the same as used in previous papers [37–39], while for the CC and NC neutrino deuteron differential cross sections relevant for SNO we use the tables given in [40]. The contribution of the cross-section uncertainties to the covariance matrix for the chlorine and gallium experiments is calculated as suggested in Ref. [32]. For a given experiment (chlorine or gallium) we use full correlation of the error on the cross section for low-energy neutrino fluxes (*pp*, *pep*, Be, N, and O), but no correlation of the cross section error between the low-energy fluxes and the higher-energy ^{8}B flux.

The neutrino survival probability P_{ee} is extracted from the neutrino evolution operator $\mathbf{U}$, which we factorize as a product of three factors $\mathbf{U}_{\rm sun}$, $\mathbf{U}_{\rm vac}$, and $\mathbf{U}_{\rm earth}$ corresponding to propagation in the Sun, vacuum, and Earth, respectively. The first and last factors include matter effects with the corresponding density profiles given in Refs. [35] and [41]. As a simplifying approximation, we assume that $\mathbf{U}_{\rm sun}$ depends only on the neutrino production point $\vec{x}_0$, $\mathbf{U}_{\rm vac}$ only on the Sun-Earth distance L, and $\mathbf{U}_{\rm earth}$ depends only on the zenith-angle ζ of the incoming neutrinos. Therefore in our calculations we neglect the small correlation between seasonal effects and day-night asymmetry [42]. For each value of the neutrino oscillation parameters $\Delta m^2_{\rm SOL}/E$, $\theta_{\rm SOL}$, and η_s we calculate the neutrino survival probability P_{ee} by averaging over $\vec{x}_0$, L, and ζ, properly accounting for all the interference terms between $\mathbf{U}_{\rm sun}$, $\mathbf{U}_{\rm vac}$, and $\mathbf{U}_{\rm earth}$.

Special care is taken in including all the theoretical and experimental errors and their cross correlations in the calculation of the covariance matrix, for which we follow the description of Ref. [31] (covariance approach). In particular, the errors associated to the boron-flux shape, the energy-scale, and the energy-resolution uncertainties of the Super-Kamiokande and SNO experiments are recalculated for each point in parameter space.

C. Results and discussion

In order to determine the expected event numbers for the various solar neutrino experiments we calculate the ν_e survival probability for each point in parameter space of $(\tan^2\theta_{\rm SOL}, \Delta m^2_{\rm SOL}, \eta_s)$ and convolute it with the standard solar model neutrino fluxes [35] and the relevant neutrino cross sections. We have compared such expected event numbers with the data described above, taking into account the detector characteristics and appropriate response functions. Using the above-mentioned $\chi^2_{\rm SOL}$ we have performed a global fit of solar neutrino data, whose results we now summarize.

Our global best fit point occurs for the values

$$\tan^2\theta_{\rm SOL}=0.46, \quad \Delta m^2_{\rm SOL}=6.6\times10^{-5}\ \ {\rm eV}^2 \qquad (3)$$

and corresponds to $\eta_s=0$. We obtain a $\chi^2_{\rm min}=65.8$ for $81-3$ degrees of freedom (DOF), leading to the excellent goodness of fit of 84%. In Fig. 1 we display the regions of solar neutrino oscillation parameters for 3 DOF with respect to this global minimum, for the standard case of active oscillations, $\eta_s=0$, as well as for $\eta_s=0.2$ and $\eta_s=0.5$. The first thing to notice is the impact of the SNO NC, spectral, and day/night data in improving the determination of the oscillation parameters: the shaded regions after their inclusion are much smaller than the hollow regions delimited by the corresponding $\rm SNO^{rate}_{CC}$ confidence contours. Especially important is the full $\rm SNO^{SP,DN}_{CC,NC}$ information for excluding *maximal* solar mixing in the LMA region and in closing the LMA region from above in $\Delta m^2_{\rm SOL}$. Values of $\Delta m^2_{\rm SOL} > 10^{-3}$ eV^2 appear only at 3σ. Previously solar data on its

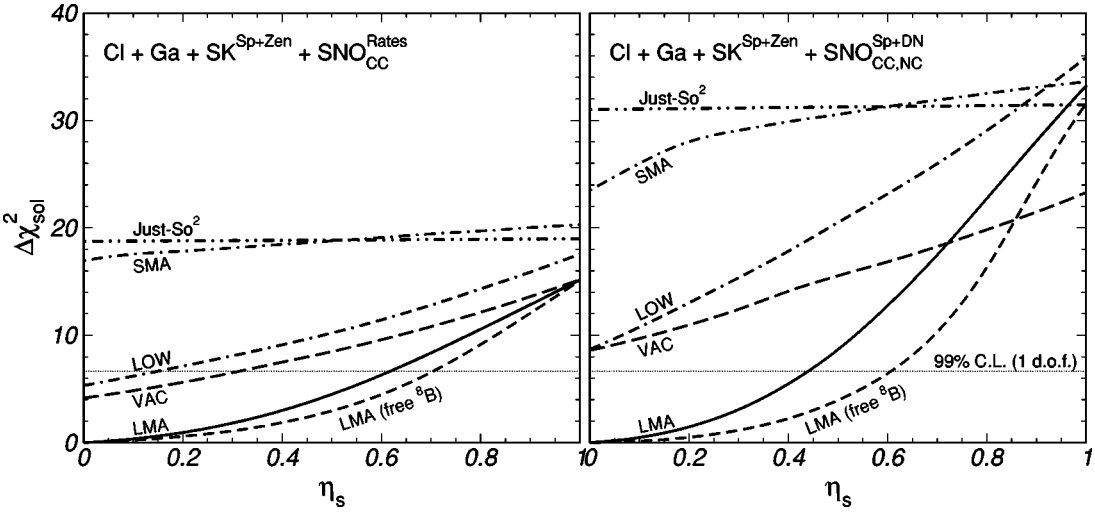

FIG. 3. $\Delta\chi^2_{\rm SOL}$ displayed as a function of η_s with respect to favored active LMA solution, for the $\mathrm{SNO}^{\rm rate}_{\rm CC}$(left panel) and the $\mathrm{SNO}^{\rm SP,DN}_{\rm CC,NC}$(right panel) analysis, as defined in text.

own could not close the LMA region, only the inclusion of data from reactor experiments [15] ruled out the upper part of the LMA region [38]. We obtain the following 3σ ranges (1 DOF):

$$\text{LMA:}\quad 0.26 \leqslant \tan^2\theta_{\rm SOL} \leqslant 0.85,$$

$$2.6\times10^{-5}\ \text{eV}^2 \leqslant \Delta m^2_{\rm SOL} \leqslant 3.3\times10^{-4}\ \text{eV}^2. \qquad (4)$$

It is interesting to note that these 3σ intervals are essentially unchanged if we minimize with respect to η_s or if we apply the constraint $\eta_s=0$ (pure active oscillations). In order to compare our allowed regions given in Fig. 1 with those of other groups, one has to take into account that we calculate the C.L. regions for the 3 DOF $\tan^2\theta_{\rm SOL}$, $\Delta m^2_{\rm SOL}$, and η_s. Therefore at a given C.L. our regions are larger than the usual regions for 2 DOF, because we also constrain the parameter η_s.

Next we notice the enhanced discrimination against non-LMA solutions implied by the new data, apparent in Figs. 1, 2, and 3. This shows that the first hints [37,43] in favor of a globally preferred LMA oscillation solution, which followed mainly from the flatness of the Super-K spectra, have now become a robust result, thanks to the additional data, to which SNO has contributed significantly.[3] One sees that, in contrast with the $\mathrm{SNO}^{\rm rate}_{\rm CC}$ situation, non-LMA solutions do not appear at 95% C.L. However, the LOW solution (LOW) and vacuum oscillation (VAC) solutions still appear at 99% C.L. for 3 DOF.

In order to concisely illustrate the above results we display in Fig. 2 the profiles of $\Delta\chi^2_{\rm SOL}$ as a function of $\Delta m^2_{\rm SOL}$ (left) as well as $\tan^2\theta_{\rm SOL}$ (right) by minimizing with respect to the undisplayed oscillation parameters, for the fixed values of $\eta_s=0$, 0.5, 1. By comparing top and bottom panels in Fig. 2 one can clearly see the impact of the full $\mathrm{SNO}^{\rm SP,DN}_{\rm CC,NC}$ sample in leading to the relative worsening of all non-LMA solutions with respect to the preferred active LMA solution.

The corresponding best fit values for the various solutions of $\Delta m^2_{\rm SOL}$ and $\theta_{\rm SOL}$ and the values of $\chi^2_{\rm SOL}$ evaluated at the best fit points are compiled in Table I. This table gives results for the three cases considered above: pure active, pure sterile, and mixed neutrino oscillations, both for the $\mathrm{SNO}^{\rm rate}_{\rm CC}$ and the full $\mathrm{SNO}^{\rm SP,DN}_{\rm CC,NC}$ analysis. To calculate the goodness of fit of the various solutions we evaluate in this table the χ^2 for $48-2$ $(81-2)$ DOF for the $\mathrm{SNO}^{\rm rate}_{\rm CC}$ ($\mathrm{SNO}^{\rm SP,DN}_{\rm CC,NC}$) analysis defined previously. Note that we fix η_s at the three values 0, 0.5, and 1. In the pure active case we find for LOW, VAC, small mixing angle (SMA), and just-so^2 the following differences in χ^2 relative to the global best fit in LMA:

$$\Delta\chi^2_{\rm LOW}=8.7,\quad \Delta\chi^2_{\rm VAC}=8.6,$$

$$\Delta\chi^2_{\rm SMA}=23.5,\quad \Delta\chi^2_{\text{just-so}^2}=31.0. \qquad (5)$$

Note that especially SMA and just-so^2 are highly disfavored with respect to LMA.

In addition to the scrutiny of the different neutrino oscillation solutions in the solar neutrino oscillation parameters $\Delta m^2_{\rm SOL}$ and $\theta_{\rm SOL}$, the present solar data can test the sterile neutrino oscillation hypothesis, characterized by the parameter η_s introduced above. The results can be presented in several equivalent ways. For example, rejection of sterile solar neutrino oscillations is already hinted by comparing the middle and right panels of Fig. 1 with the left one, corresponding to the pure active oscillation case: clearly the solutions deteriorate as η_s increases. Furthermore, the lines for $\eta_s=0.5$ and $\eta_s=1$ shown in Fig. 2 clearly show that sterile solutions are strongly disfavored with respect to pure active solutions.

In order to summarize the above results we display in Fig. 3 the profile of $\Delta\chi^2_{\rm SOL}$ as a function of $0\leqslant\eta_s\leqslant1$, irrespective of the detailed values of the solar neutrino oscillation

[3]See also Ref. [44].

TABLE I. Best fit values of $\Delta m^2_{\rm SOL}$ and $\theta_{\rm SOL}$ with the corresponding $\chi^2_{\rm SOL}$ and GOF for pure active, pure sterile, and mixed neutrino oscillations. Results are given for the $\rm SNO^{rate}_{CC}$ (left column) and for the full $\rm SNO^{SP,DN}_{CC,NC}$ analysis (right column). The relevant number of DOF is $48-2$ $(81-2)$ for the $\rm SNO^{rate}_{CC}$ $(\rm SNO^{SP,DN}_{CC,NC})$ analysis.

	$\rm SNO^{rate}_{CC}$				$\rm SNO^{SP,DN}_{CC,NC}$			
Region	$\tan^2\theta_{\rm SOL}$	$\Delta m^2_{\rm SOL}$	$\chi^2_{\rm SOL}$	GOF	$\tan^2\theta_{\rm SOL}$	$\Delta m^2_{\rm SOL}$	$\chi^2_{\rm SOL}$	GOF
				Pure active ($\eta_s=0$)				
LMA	0.46	7.2×10^{-5}	40.9	69%	0.46	6.6×10^{-5}	65.8	86%
LOW	0.83	4.8×10^{-8}	46.2	46%	0.66	7.9×10^{-8}	74.4	62%
VAC	1.7	6.6×10^{-10}	45.0	51%	1.7	6.3×10^{-10}	74.4	63%
SMA	1.1×10^{-3}	5.0×10^{-6}	57.8	11%	1.4×10^{-3}	5.0×10^{-6}	89.3	20%
just-so^2	1.0	5.5×10^{-12}	59.6	9%	1.0	5.5×10^{-12}	96.8	8%
				Mixed ($\eta_s=0.5$)				
LMA	0.46	7.6×10^{-5}	45.4	50%	0.42	6.6×10^{-5}	74.4	62%
LOW	0.91	3.5×10^{-8}	51.1	28%	0.83	4.8×10^{-8}	86.3	27%
VAC	1.6	6.9×10^{-10}	49.4	34%	0.35	4.6×10^{-10}	81.3	41%
SMA	3.6×10^{-4}	4.0×10^{-6}	59.7	8%	4.4×10^{-4}	4.0×10^{-6}	96.3	9%
just-so^2	1.0	5.5×10^{-12}	59.8	8%	1.0	5.5×10^{-12}	97.0	8%
				Pure sterile ($\eta_s=1$)				
LMA	0.44	1.6×10^{-4}	56.0	15%	0.38	1.6×10^{-4}	99.0	6%
LOW	1.6	1.4×10^{-9}	58.5	10%	1.6	1.1×10^{-9}	101.6	4%
VAC	1.7	6.9×10^{-10}	56.1	15%	0.33	4.6×10^{-10}	89.1	21%
SMA	3.5×10^{-4}	3.5×10^{-6}	61.2	7%	3.6×10^{-4}	3.5×10^{-6}	99.4	6%
just-so^2	1.1	5.5×10^{-12}	59.9	8%	1.0	5.5×10^{-12}	97.2	8%

parameters $\Delta m^2_{\rm SOL}$ and $\theta_{\rm SOL}$. This figure clearly illustrates the degree with which the solar neutrino data sample rejects the presence of a sterile component for each one of the possible solar neutrino oscillation solutions. The figure shows how the preferred LMA status survives in the presence of a small sterile component characterized by η_s (also seen in Figs. 1 and 2). Further, one sees that the value $\eta_s=0$ is always preferred, so that increasing η_s leads to a deterioration of all oscillation solutions. Notice that there is a crossing between the LMA and VAC solutions, as a result of which the best pure sterile description lies in the vacuum regime. However, in the global analysis pure sterile oscillations with $\eta_s=1$ are highly disfavored. We find a χ^2-difference between pure active and sterile of $\Delta\chi^2_{\rm s-a}=33.2$ if we restrict to the LMA solution, or $\Delta\chi^2_{\rm s-a}=23.3$ if we allow also for VAC. For 3 DOF the $\Delta\chi^2_{\rm s-a}=23.3$ implies that pure sterile oscillations are ruled out at 99.997% C.L. compared to the active case.

For the LMA solution we have also performed an analysis without fixing the boron flux to its SSM prediction. In this case we treat the ^{8}B flux as a free parameter in the fit, and remove the error on this flux from the covariance matrix. From Fig. 3 one can see that the constraint on η_s is weaker in the boron-free case than in the boron-fixed one, since a *small* sterile component can now be partially compensated by increasing the total ^{8}B flux coming from the Sun. From the figure we obtain the bounds

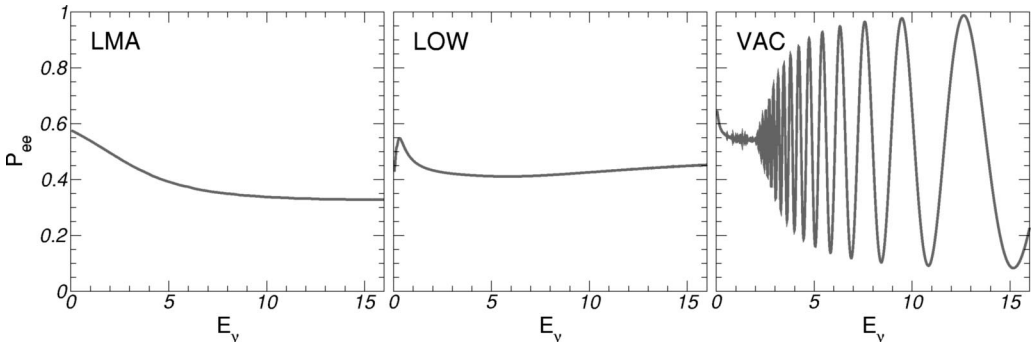

FIG. 4. Best-fit active solar neutrino survival probabilities.

$$\text{solar data:} \quad \eta_s \leq 0.44 \ \text{(boron-fixed)}, \qquad \eta_s \leq 0.61 \ \text{(boron-free)} \tag{6}$$

at 99% C.L. for 1 DOF. In summary, we have found that, as long as the admixture of sterile neutrinos is acceptably small, the LMA is always the best of the oscillation solutions, establishing its robustness also in our generalized oscillation scheme.

To round off our discussion of the solar neutrino fit update we present in Fig. 4 the ν_e survival probability versus energy E for the various solutions LMA, LOW, and VAC, calculated as described above at the local χ^2-minima given in Table I. Similar plots can be made for the case of sterile oscillations.

D. Comparison with other groups

Before turning to the atmospheric neutrino fits let us compare our solar neutrino results with those of other groups. Since the release of the latest SNO data in April 2002 several analyses have appeared. Taking into account the large amount of experimental input data, variations in the analysis (such as the construction of the χ^2 function or the treatment of theoretical errors) and the complexity of the codes involved it seems interesting to compare quantitatively the outcomes of different analyses. In Table II we have compiled some illustrative results of the solar neutrino analyses performed by the SNO and Super-K collaborations [1,7], as well as theoretical ones [9,25–31].

Generally speaking, on statistical grounds, one expects the differences in the statistical treatment of the data to have little impact on the global best fit parameter values, which lie in the LMA region for all analyses and are in good agreement. These differences typically become more visible as one compares absolute values of the χ^2, and/or as one departs from the best fit region towards more disfavored solutions. Aware of this, we took special care with details such as the dependence of the theoretical errors on the oscillation parameters, which enter in the covariance matrix characterizing the Super-K and SNO electron recoil spectra. This way we obtain results which we consider reliable in the full oscillation parameter space.

In the row labeled ''DOF'' we show the number of analyzed data points minus the fitted parameters in each analysis.[4] One can see from these numbers that various groups use different experimental input data, in particular the spectral and zenith angle information of Super-K and/or SNO is treated in different ways. Despite obvious differences in the analyses there is relatively good agreement on the best fit LMA active oscillation parameters: the obtained best fit values for $\tan^2\theta_{\rm SOL}$ are in the range $0.34-0.47$ and for $\Delta m^2_{\rm SOL}$ they lie in the interval $(5.0-7.9)\times 10^{-5}$ eV^2. There is also good agreement on the allowed ranges of the oscillation parameters (not shown in the table). For example, the 3σ intervals given in Ref. [25] ($0.24 \leq \tan^2\theta_{\rm SOL} \leq 0.89$ and 2.3×10^{-5} eV$^2 \leq \Delta m^2_{\rm SOL} \leq 3.7\times 10^{-4}$ eV^2) and in Ref. [29] ($\tan^2\theta_{\rm SOL} \leq 0.84$ and 2.3×10^{-5} eV$^2 \leq \Delta m^2_{\rm SOL} \leq 3.6\times 10^{-4}$ eV^2) agree very well with the ranges given in Eq. (4). However, even for the favored LMA solution, there are some differences in the GOF of the best fit LMA solution, ranging from 53% [25] to 97% [27], due to differences in the construction of the χ^2 function by different groups.

There is remarkable agreement on the rejection of the LOW solution with respect to LMA with a $\Delta\chi^2_{\rm LOW,active} \approx 10$. Our result for the vacuum solution $\Delta\chi^2_{\rm VAC,active}=8.6$ is in good agreement with the values obtained in Refs. [1,25,29,31], whereas Refs. [26,27,30] obtain higher values. Our result for the SMA solution of $\Delta\chi^2_{\rm SMA,\ active}=23.5$ is in good agreement with the values obtained in Refs. [25,30,31]; while Refs. [26,29] and especially Ref. [27] obtain higher values. On the other hand in Ref. [1] SMA is somewhat less disfavored.[5]

There had been so-far no dedicated global analysis of solar neutrino oscillations including the most recent SNO data for the case where sterile neutrinos take part in solar oscillations ($\eta_s \neq 0$). Model-independent considerations of transitions into sterile neutrinos can be found in Refs. [6,26–28]. Solar neutrino oscillations in the presence of active-sterile admixtures are also studied in Ref. [32], although in a different context. In the lower part of Table II we compare the partial results given in Refs. [25] and [30] for the pure sterile case ($\eta_s=1$) with the corresponding values found in the present analysis. Although there are noticeable differences of the shown $\Delta\chi^2$ values, there is agreement on the qualitative behavior. We have also studied intermediate levels of sterile neutrino admixture, giving the corresponding regions of oscillation parameters and the full χ^2 profiles relative to the favored active LMA solution (not shown in Table II, see Figs. 1, 2, and 3).

We now turn to the analysis of the latest atmospheric data. As already mentioned in the introduction, separate analyses of solar and atmospheric data samples constitute the necessary ingredients towards a full combined study of all current oscillation data, including also the short-baseline data, as shown in [23,24].

III. ATMOSPHERIC NEUTRINOS

A. Active-sterile atmospheric neutrino oscillations

In our analysis of atmospheric data we will make use of the hierarchy $\Delta m^2_{\rm SOL} \ll \Delta m^2_{\rm ATM}$ and neglect the solar mass splitting. Further, in order to comply with the strong constraints from reactor experiments [15] we completely decouple the electron neutrino from atmospheric oscillations.[6] In the following we will consider atmospheric neutrino data in a generalized oscillation scheme in which a light sterile neutrino takes part in the oscillations. The setting for such scenarios are four-neutrino mass schemes [16–18]. In such schemes, besides the solar and atmospheric mass-splittings,

[4]Here we do not treat η_s as a free fit parameter, since we consider only the limiting cases $\eta_s=0$ and 1; this is the reason for the number $81-2$ in the present analysis.

[5]Tracing back the reason for these and other differences in Table II goes beyond the scope of this work.

[6]For a dedicated study of these issues see Ref. [45].

TABLE II. Comparison of solar neutrino analyses among different groups. We show the number of analyzed data points minus the fitted parameters, the best fit values of $\tan^2\theta_{\mathrm{SOL}}$ and $\Delta m^2_{\mathrm{SOL}}$ for active oscillations and the corresponding χ^2-minima, and GOF. Further we show the $\Delta\chi^2$ with respect to the best fit LMA active solution for various other solutions (active, as well as sterile).

	SNO Collaboration [7], Table IV	Super-K Collaboration [1], Table III	Barger *et al.* [27], Table II	Bandyopadhyay *et al.* [26], Table II	Bahcall *et al.* [25], Table IV	Creminelli *et al.* [30], Chap. 7	Aliani *et al.* [28], Table II	De Holanda and Smirnov [29], Table I	Fogli *et al.* [31], Table I	Barranco *et al.* [9], Table I	Present analysis
DOF	75−3	46	75−3	49−4	80−3	49−2	41−4	81−3	81−3	81−2	81−2
Best fit						LMA solution					
$\tan^2\theta_{\mathrm{SOL}}$	0.34	0.38	0.39	0.41	0.45	0.45	0.40	0.41	0.42	0.47	0.46
$\Delta m^2_{\mathrm{SOL}}$ $[10^{-5}$ eV$^2]$	5.0	6.9	5.6	6.1	5.8	7.9	5.4	6.1	5.8	5.6	6.6
χ^2_{LMA}	57.0	43.5	50.7	40.6	75.4	33.0	30.8	65.2	73.4	68.0	65.8
GOF	90%	58%	97%	66%	53%	94%	80%	85%	63%	81%	86%
$\Delta\chi^2_{\mathrm{LOW,active}}$	10.7	9.0	9.2	10.0	9.6	8.1		12.4	10.0		8.7
$\Delta\chi^2_{\mathrm{VAC,active}}$		10.0	25.6	15.5	10.1	14.0		9.7	7.8		8.6
$\Delta\chi^2_{\mathrm{SMA,active}}$		15.4	57.3	30.4	25.6	23.0		34.5	23.5		23.5
$\Delta\chi^2_{\mathrm{LMA,sterile}}$						29.0					33.2
$\Delta\chi^2_{\mathrm{LOW,sterile}}$											35.9
$\Delta\chi^2_{\mathrm{VAC,sterile}}$					26.0						23.3
$\Delta\chi^2_{\mathrm{SMA,sterile}}$					39.7						33.6

there is also a large Δm^2 motivated by the LSND experiment [22]. In contrast with the case of solar ν_e oscillations, the constraints on the ν_μ content in atmospheric oscillations are not so stringent: in fact such constrains are provided by atmospheric data themselves [46]. As a result, to describe atmospheric neutrino oscillations in this general framework [23,33] we need two more parameters besides the standard 2-neutrino oscillation parameters $\theta_{\rm ATM}$ and $\Delta m^2_{\rm ATM}$. We will use the parameters d_μ and d_s already introduced in Ref. [23], and defined in such a way that $(1-d_\mu)$ and $(1-d_s)$ correspond to the fractions of ν_μ and ν_s participating in oscillations with $\Delta m^2_{\rm ATM}$, respectively. Hence pure active atmospheric oscillations with $\Delta m^2_{\rm ATM}$ are recovered in the limit $d_\mu=0$ and $d_s=1$. In four-neutrino models there is a mass scheme-dependent relationship between d_s and the solar parameter η_s. For details see Ref. [23].

We will also perform an analysis by imposing the constraint $d_\mu=0$. In such ''restricted'' analysis the ν_μ is completely constrained to the atmospheric mass states. Only in this limit the parameter d_s has a similar interpretation as η_s introduced in the solar case. For $d_\mu=0$ we obtain that ν_μ oscillates into a linear combination of ν_τ and ν_s with $\Delta m^2_{\rm ATM}$:

$$d_\mu=0: \quad \nu_\mu \to \sqrt{d_s}\,\nu_\tau + \sqrt{1-d_s}\,\nu_s. \tag{7}$$

B. Data and analysis

For the atmospheric data analysis we use all the charged-current data from the Super-Kamiokande [13] and MACRO [14] experiments. The Super-Kamiokande data include the e-like and μ-like data samples of sub- and multi-GeV contained events (ten bins in zenith angle), as well as the stopping (five angular bins) and through-going (ten angular bins) up-going muon data events. We do not use the information on ν_τ appearance, multiring μ, and neutral-current events since an efficient Monte Carlo simulation of these data samples would require a more detailed knowledge of the Super-Kamiokande experiment, and in particular of the way the neutral-current signal is extracted from the data. Such information is presently not available to us. From MACRO we use the through-going muon sample divided in ten angular bins [14]. We did not include in our fit the results of other atmospheric neutrino experiments, such as the recent 5.9 kton-yr data from Soudan-2 [47], since at the moment the statistics is completely dominated by Super-Kamiokande [38]. Furthermore, some of the older experiments have no angular sensitivity, and thus cannot be used to discriminate between active and sterile neutrino conversion, our main goal.

Our statistical analysis of the atmospheric data is similar to that used in Ref. [23], except that we now take advantage of the new Super-Kamiokande data and of the full ten-bin zenith-angle distribution for the contained events, rather than the five-bin distribution employed previously. Therefore we have now 65 observables, which we fit in terms of the four relevant parameters $\Delta m^2_{\rm ATM}$, $\theta_{\rm ATM}$, d_μ, and d_s:

$$\chi^2_{\rm ATM}(\Delta m^2_{\rm ATM}, \theta_{\rm ATM}, d_\mu, d_s) = \sum_{i,j=1}^{65} (N_i^{ex}-N_i^{th})\cdot(\sigma^2_{ex}+\sigma^2_{th})^{-1}_{ij}\cdot(N_j^{ex}-N_j^{th}). \tag{8}$$

Concerning the theoretical Monte Carlo program, we improve the method presented in Ref. [38] by properly taking into account the scattering angle between the incoming neutrino and the scattered lepton directions. This was already the case for sub-GeV contained events, however, previously [23] we made the simplifying assumption of full neutrino-lepton collinearity in the calculation of the expected event numbers for the multi-GeV contained and up-going-μ data samples. While this approximation is still justified for the stopping and thru-going muon samples, in the multi-GeV sample the theoretically predicted value for down-coming ν_μ is systematically higher if full collinearity is assumed. The reason for this is that the strong suppression observed in these bins cannot be completely ascribed to the oscillation of the down-coming neutrinos (which is small due to small travel distance). Because of the non-negligible neutrino-lepton scattering angle at these multi-GeV energies there is a sizable contribution from up-going neutrinos (with a higher conversion probability due to the longer travel distance) to the down-coming leptons. However, this problem is less visible when the angular information of multi-GeV events is included in a five angular bins presentation of the data, as previously assumed [48].

C. Results and Discussion

Folding together the atmospheric neutrino fluxes [49], our calculated neutrino survival probabilities including Earth matter effects with the profile of Ref. [41], and the relevant neutrino cross sections, we determine the expected event numbers for the various atmospheric neutrino observables,

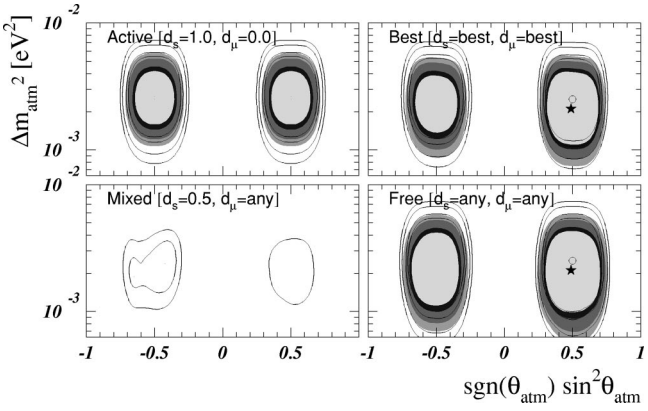

FIG. 5. Allowed regions of the parameters $\sin^2\theta_{\rm ATM}$ and $\Delta m^2_{\rm ATM}$ at 90%, 95%, 99%, and 3σ for 4 DOF and different assumptions on the parameters d_s and d_μ (see text). The lines (shaded regions) correspond to 1289 (1489) days of Super-K data.

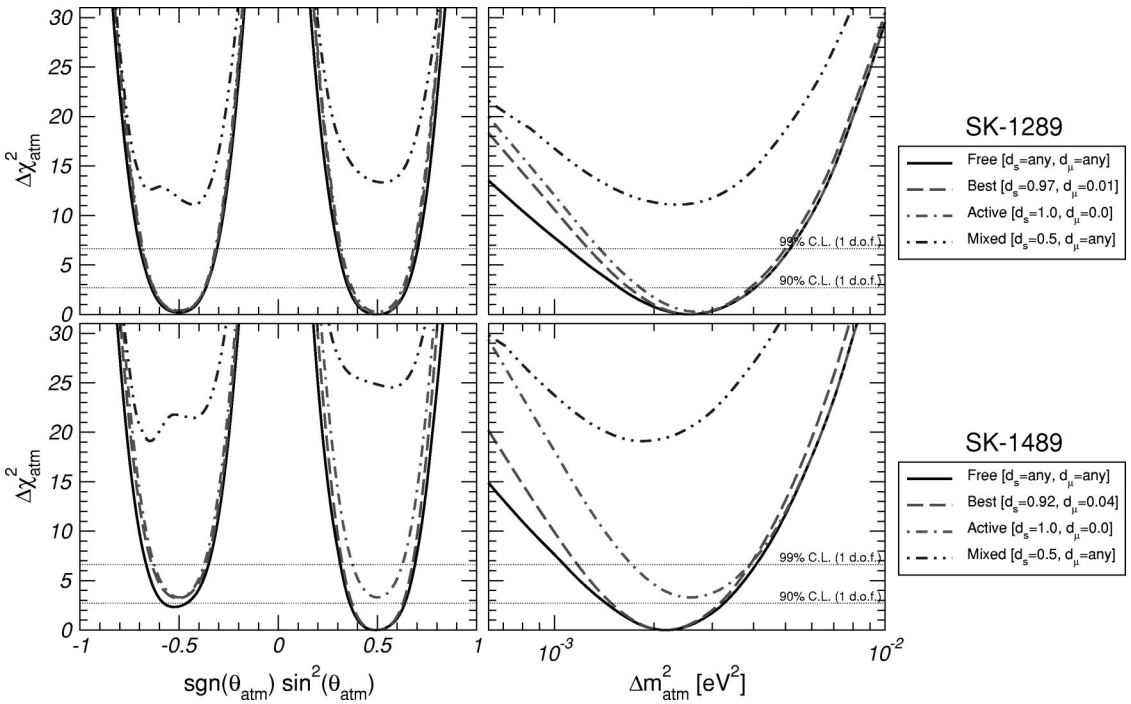

FIG. 6. $\Delta\chi^2_{\rm ATM}$ as a function of $\sin^2\theta_{\rm ATM}$ (left) and $\Delta m^2_{\rm ATM}$ (right), using 1289-(upper) and 1489-(lower) days of Super-K data, for the case of neutrino oscillations with arbitrary d_s and d_μ, best-fit d_s and d_μ, pure active, and mixed active-sterile neutrino oscillations.

taking into account the appropriate detector response characteristics. Comparing with the data described in Sec. III B, we have performed a global fit of the atmospheric neutrino data using the above-discussed $\chi^2_{\rm ATM}$, following the same method used in Ref. [38]. We now summarize the main features of this fit.

Our global best fit point occurs at the parameter values

$$\sin^2\theta_{\rm ATM}=0.49,\ \ \Delta m^2_{\rm ATM}=2.1\times10^{-3}\ {\rm eV}^2\ \ \ ({\rm best}) \tag{9}$$

and $d_s=0.92$, $d_\mu=0.04$. We see that atmospheric data prefers a small sterile neutrino admixture. However, this effect is not statistically significant, also the pure active case ($d_s=1, d_\mu=0$) gives an excellent fit: the difference in χ^2 with respect to the best fit point is only $\Delta\chi^2_{\rm act-best}=3.3$. For the pure active best fit point we obtain

$$\sin^2\theta_{\rm ATM}=0.5,\ \ \Delta m^2_{\rm ATM}=2.5\times10^{-3}\ {\rm eV}^2\ \ \ ({\rm active}) \tag{10}$$

with the 3σ ranges (1 DOF)

$$0.3\leqslant\sin^2\theta_{\rm ATM}\leqslant0.7,$$

$$1.2\times10^{-3}\ {\rm eV}^2\leqslant\Delta m^2_{\rm ATM}\leqslant4.8\times10^{-3}\ {\rm eV}^2\quad({\rm active}). \tag{11}$$

The determination of the parameters $\theta_{\rm ATM}$ and $\Delta m^2_{\rm ATM}$ is summarized in Figs. 5 and 6. At a given C.L. we cut the $\chi^2_{\rm ATM}$ at a $\Delta\chi^2$ determined by 4 DOF to obtain four-dimensional volumes in the parameter space of $(\theta_{\rm ATM},\Delta m^2_{\rm ATM},d_\mu,d_s)$. In the upper panels we show sections of these volumes at values of $d_s=1$ and $d_\mu=0$ corresponding to the pure active case (left) and at the best fit point (right). Again we observe that moving from pure active to the best fit does not change the fit significantly. In the lower right panel we project away both d_μ and d_s, whereas in the lower left panel we fix $d_s=0.5$ and project away only d_μ. Comparing the regions resulting from 1489-days Super-K data (shaded regions) with those from the 1289-days Super-K sample (hollow regions) we note that the new data leads to a slightly better determination of $\theta_{\rm ATM}$ and $\Delta m^2_{\rm ATM}$. However, more importantly, from the lower left panel we see that the new data shows a stronger rejection against a sterile admixture: for $d_s=0.5$ no allowed region appears at 3σ for 4 DOF.

In Fig. 6 we display the $\Delta\chi^2$ with respect to the global best fit point as a function of $\sin^2\theta_{\rm ATM}$ (for both signs of $\theta_{\rm ATM}$) and $\Delta m^2_{\rm ATM}$, minimizing with respect to the other parameter, for different assumptions on the parameters d_s and d_μ. In contrast to the solar case shown in Fig. 2 the atmospheric χ^2 exhibits a beautiful quadratic behavior, reflecting the fact that the oscillation solution to the atmospheric neutrino problem is robust and unique. Notice again the significant worsening of the fit for the case of a sizable sterile neutrino admixture (see, e.g., the line corresponding to $d_s=0.5$).

In Fig. 7 we summarize the behavior of atmospheric χ^2 with respect to the parameters d_s and d_μ. Indeed, the most striking result of the present improved analysis is the stronger rejection we now obtain on the fraction of the sterile neutrino $1-d_s$ in atmospheric oscillations. Figure 7(b) clearly illustrates the degree to which the atmospheric neutrino

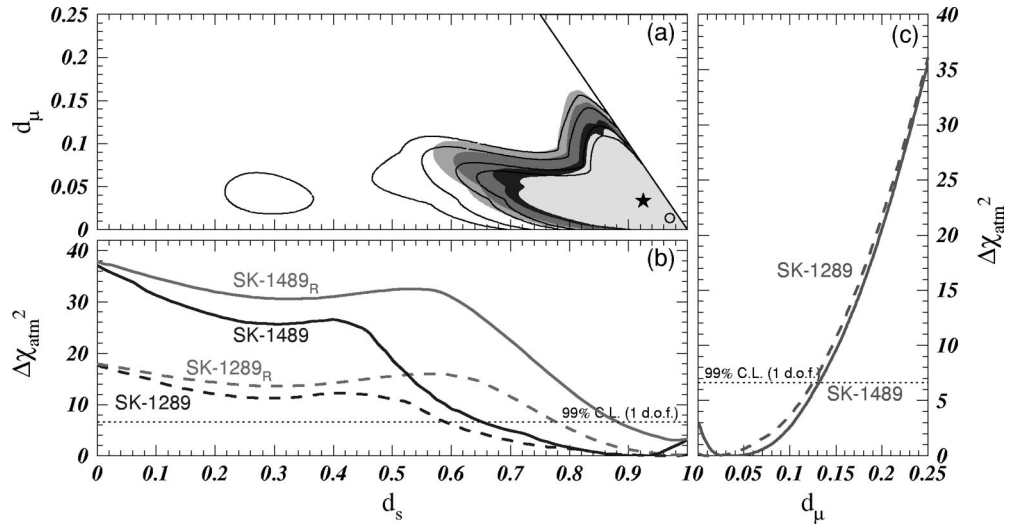

FIG. 7. (a) Allowed regions of the parameters d_s and d_μ at 90%, 95%, 99%, and 3σ for 2 DOF. The lines (shaded regions) correspond to 1289-(1489-) days Super-K data. Further we show $\Delta\chi^2_{\rm ATM}$ as a function of d_s (b) and d_μ (c), minimized with respect to all other parameters. The subscript "R" refers to the restricted analysis with $d_\mu=0$.

data sample rejects the presence of a sterile component. On this basis one can place a model-independent atmospheric limit on the parameter d_s,

$$\text{atmospheric data:} \quad 1-d_s \leqslant 0.35 \tag{12}$$

at 99% C.L. (1 DOF). For the case of the restricted analysis, in which $d_\mu=0$, we obtain[7]

$$d_\mu=0: \quad 1-d_s \leqslant 0.16. \tag{13}$$

By comparing Eqs. (12) and (13) we note the importance of taking into account the finite d_μ value in the analysis.

Although there is no substantial change in the 99% C.L. bounds on $1-d_s$ due to the new Super-K data there is a huge effect for the case of sizable sterile neutrino admixtures, $d_s \leqslant 0.5$. In Table III we have compiled the best fit values of $\sin^2\theta_{\rm ATM}$, $\Delta m^2_{\rm ATM}$, the χ^2 values, and the GOF for the various atmospheric data samples for pure active and pure sterile oscillations. In the last column we give the difference in χ^2 between active and sterile oscillation cases. Comparing these numbers for the 1289- and 1489-days Super-K samples we observe that all the new data except the sub-GeV sample lead to a significantly higher rejection against sterile oscillations. In combination with MACRO data the 1289-days Super-K gave a difference between pure sterile and active oscillations of $\Delta\chi^2_{\rm s-a}=17.8$, whereas with the recent data we obtain

$$\Delta\chi^2_{\rm s-a}=34.6, \tag{14}$$

showing that pure sterile oscillations are highly disfavored with respect to the active ones.[8] Let us note that MACRO data give an important contribution to this effect: MACRO alone disfavors the sterile oscillations already with $\Delta\chi^2_{\rm s-a}=9.0$. These limits on the sterile admixture are significantly stronger than obtained previously [23] and play an important role in ruling out four-neutrino oscillation solutions in a combined global analysis of the LSND anomaly [24]. Note, however, that in contrast with the case of d_s, there is no substantial improvement in constraining the parameter d_μ due to the new data, as seen in Fig. 7 (c).

In order to better appreciate the excellent quality of the neutrino oscillation description of the present atmospheric neutrino data sample we display in Fig. 8 the zenith angle distribution of atmospheric neutrino events. Clearly, active neutrino oscillations describe the data very well indeed. In contrast, no oscillations can be visually spotted as being inconsistent. On the other hand conversions to sterile neutrinos lead to an excess of events for neutrinos crossing the core of the Earth, in all the data samples except sub-GeV.

D. Comparison with other groups

Let us briefly compare our atmospheric neutrino oscillation results with those of other groups. Apart from the analyses presented in Refs. [23,33] there had been no other complete atmospheric neutrino analysis taking into account the

[7]Note that in this case the C.L. regions should be defined with respect to the "restricted" best fit point, which occurs for $d_s=0.99$, and not with respect to the global one.

[8]Here we should remark that this big improvement in constraining the sterile component—which is clearly visible also in the analyses presented by the Super-K collaboration itself—cannot be explained *only* by the improved statistics provided by the new data sample. The leading contribution comes instead from a change in the data themselves, which may indicate that some modification in the experimental efficiencies has been introduced. However, we have verified that such changes do not affect the theoretical prediction, since no difference between 1289 and 1489 days is visible in the Monte Carlo program of the Super-K collaboration.

TABLE III. Atmospheric neutrino best-fit oscillation parameters for pure active and pure sterile oscillations for the various data samples.

		Active ($d_\mu=0$, $d_s=1$)				Sterile ($d_\mu=0$, $d_s=0$)				
Data sample	DOF	$\sin^2\theta$	Δm^2 [eV^2]	$\chi^2_{\rm act}$	GOF	$\sin^2\theta$	Δm^2 [eV^2]	$\chi^2_{\rm ste}$	GOF	$\Delta\chi^2_{\rm s-a}$
Super-K-1289 days, improved										
SK sub-GeV	20−2	0.50	2.1×10^{-3}	14.9	67%	0.50	2.2×10^{-3}	15.0	66%	0.1
SK multi-GeV	20−2	0.50	1.8×10^{-3}	6.4	99%	0.57	3.5×10^{-3}	11.3	88%	4.8
SK stop-μ	5−2	0.50	4.2×10^{-3}	1.2	76%	0.61	4.0×10^{-3}	3.1	38%	1.9
SK thru-μ	10−2	0.29	6.3×10^{-3}	5.3	73%	0.84	1.0×10^{-2}	7.8	45%	2.5
MACRO	10−2	0.50	2.4×10^{-3}	11.0	20%	0.96	9.4×10^{-3}	20.0	1%	9.0
SK contained	40−2	0.50	2.0×10^{-3}	21.4	99%	0.54	3.0×10^{-3}	26.9	91%	5.5
Upgoing-μ	25−2	0.50	3.3×10^{-3}	19.2	69%	0.72	4.2×10^{-3}	32.8	8%	13.6
SK+MACRO	65−2	0.50	2.7×10^{-3}	41.7	98%	0.56	2.8×10^{-3}	59.4	60%	17.8
Super-K-1489 days										
SK sub-GeV	20−2	0.50	1.9×10^{-3}	9.0	96%	0.51	2.0×10^{-3}	9.0	96%	0.0
SK multi-GeV	20−2	0.50	1.3×10^{-3}	10.2	93%	0.57	3.5×10^{-3}	18.4	43%	8.2
SK stop-μ	5−2	0.50	2.8×10^{-3}	1.5	69%	0.75	2.8×10^{-3}	6.9	8%	5.4
SK thru-μ	10−2	0.50	3.5×10^{-3}	6.3	61%	0.84	6.7×10^{-3}	16.0	4%	9.7
MACRO	10−2	0.50	2.4×10^{-3}	11.0	20%	0.96	9.4×10^{-3}	20.0	1%	9.0
SK contained	40−2	0.50	1.5×10^{-3}	19.3	99%	0.54	3.0×10^{-3}	28.1	88%	8.8
Upgoing-μ	25−2	0.50	3.0×10^{-3}	18.9	71%	0.75	3.2×10^{-3}	40.8	1%	22.0
SK+MACRO	65−2	0.50	2.5×10^{-3}	40.2	99%	0.61	2.7×10^{-3}	74.9	15%	34.6

most general structure of neutrino mixing in the presence of sterile neutrinos, characterized by four mixing parameters. In the analyses of Refs. [13,50] the ν_μ is restricted to the atmospheric mass states, which corresponds to the constraint $d_\mu=0$ in our parametrization. However, at the corresponding limiting cases our generalized analysis can be compared with the results of other works. Let us further note that the analysis of Ref. [50] is based on the 1289-days SK data sample (79.5 kton yr) and in contrast to Refs. [13,50] we use also data from the MACRO experiment.

First, we find very good agreement in the case of pure active oscillations: the agreement of our best fit values given

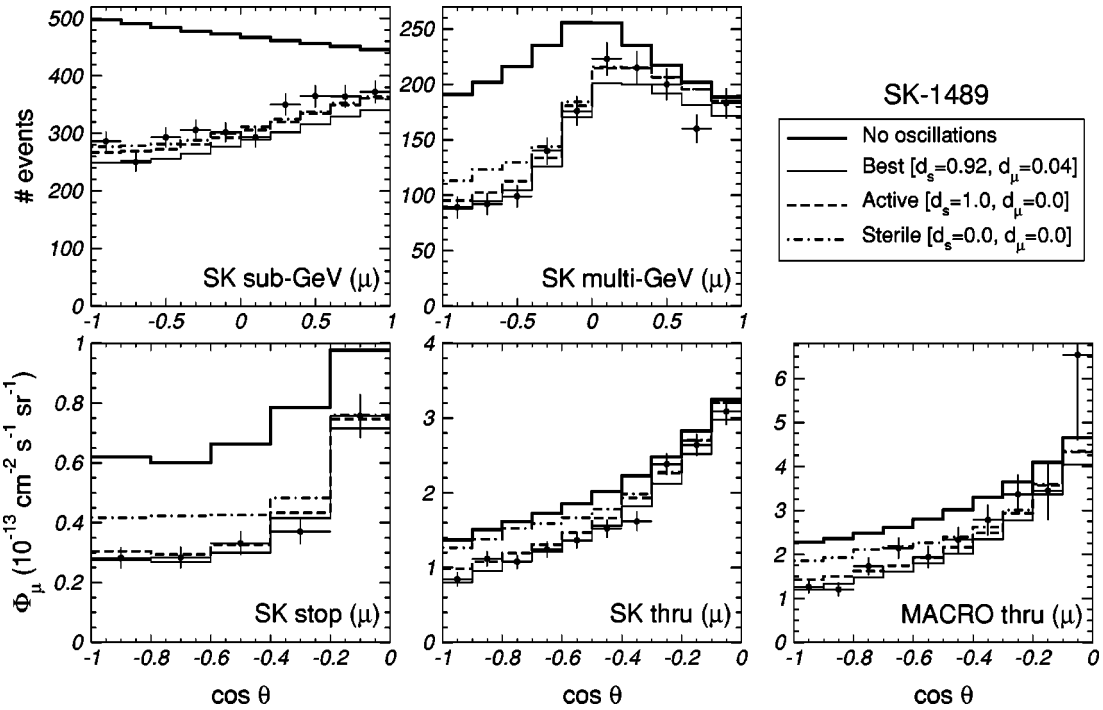

FIG. 8. Zenith angle dependence of the μ-like data used in our fit. Further we show the predicted number of atmospheric neutrino events for best-fit, pure-active, and pure-sterile oscillations, and no oscillations.

in Eq. (10) with those obtained by the Super-K Collaboration ($\sin^2\theta_{\rm ATM}=0.5$, $\Delta m^2_{\rm ATM}=2.5\times10^{-3}$ eV^2 [13]) is excellent, with good agreement also with the results of Ref. [50] ($\sin^2\theta_{\rm ATM}=0.41$, $\Delta m^2_{\rm ATM}=3\times10^{-3}$ eV^2). Similarly, also the allowed ranges shown in the upper left panel of Fig. 5 compare very well with the ranges obtained in Refs. [13,50]. This shows that the determination of the active atmospheric oscillation parameters is already rather stable with respect to variations in the analysis and inclusion of additional data. Concerning admixtures of sterile neutrinos, we note that it is presently not possible to use information on ν_τ appearance, multiring μ, and neutral-current events outside the Super-K Collaboration because to simulate these data a detailed knowledge of the detector and the applied cuts is necessary. These classes of events should provide additional sensitivity towards rejecting a possible contribution of sterile neutrinos. Therefore the fact that the value of $\Delta\chi^2_{\rm s-a}=49.8$ [13] between pure active and sterile oscillations obtained by the Super-K Collaboration is higher than our value 34.6 given in Eq. (14) is understandable, since with the Super-K data accessible to us we have a reduced discrimination between active and sterile oscillations, based solely on the matter effects.

IV. CONCLUSIONS

Prompted by the recent data on solar and atmospheric neutrinos we have reanalyzed the global status of oscillation solutions, taking into account that both the solar ν_e and the atmospheric ν_μ may convert to a mixture of active and sterile neutrinos. In addition to the SNO neutral current, spectral, and day/night ($\rm SNO^{SP,DN}_{CC,NC}$) results we add the latest 1496-day solar and 1489-day atmospheric Super-K neutrino data samples.

We have studied the impact of the recent solar data in the determination of the regions of oscillation parameters for different allowed η_s values, displaying the global behavior of $\Delta\chi^2_{\rm SOL}(\Delta m^2_{\rm SOL})$ and $\Delta\chi^2_{\rm SOL}(\theta_{\rm SOL})$, calculated with respect to the favored active LMA solution. We have investigated in detail the impact of the full Cl + Ga rates + Super-K spectra + the complete $\rm SNO^{SP,DN}_{CC,NC}$ data set, comparing with the situation when this year's SNO data is left out. We confirm the clear preference for the LMA solution of the solar neutrino problem and obtain that the LOW, VAC, SMA, and just-so^2 solutions are disfavored with a $\Delta\chi^2=9$, 9, 23, and 31, respectively, for the pure active case. In addition, we find that the global solar data sample constrains admixtures of a sterile neutrino to be smaller than 44% at 99% C.L. This bound is relaxed to 61% when the solar ^{8}B flux is treated as a free parameter. A pure sterile solution is ruled out with respect to the active one at 99.997% C.L. For allowed sterile neutrino admixtures LMA is always the best of all the oscillation solutions. We remark, however, the existence of nonoscillation solutions [8–10]. These will be crucially tested [9,51] at the up-coming KamLAND reactor experiment [52].

By performing an improved fit of the atmospheric data, we have also updated the corresponding regions of oscillation parameters for the case where the atmospheric ν_μ convert to a mixture of active and sterile neutrinos. We have displayed the global behavior of $\Delta\chi^2_{\rm ATM}(\Delta m^2_{\rm ATM})$ and $\Delta\chi^2_{\rm ATM}(\theta_{\rm ATM})$ for different allowed values of the sterile neutrino admixture in the atmospheric channel. We have compared the situation before and after the recent 1489-day atmospheric Super-K data samples and have shown that the GOF of the oscillation hypothesis is excellent. We have found that the recent 1489-day atmospheric Super-K data strongly constrain a sterile component in atmospheric oscillations: if the ν_μ is restricted to the atmospheric mass states only a sterile admixture of 16% is allowed at 99% C.L., while a bound of 35% is obtained in the unconstrained case. Pure sterile oscillations are disfavored with a $\Delta\chi^2=34.6$ compared to the active case.

ACKNOWLEDGMENTS

We thank Mark Chen, Andre Hamer, Art McDonald, and Scott Oser for help in accessing the details of the SNO experiment needed for our analysis. This work was supported by Spanish grant BFM2002-00345, by the European Commission RTN network HPRN-CT-2000-00148, and by the European Science Foundation network grant No. 86. T.S. has been supported by the Austrian Academy of Science and, in the early stages of this work, by the European Commission Research Training Site contract HPMT-2000-00124 of the host group. M.M. was supported by contract HPMF-CT-2000-01008 and M.A.T. was supported by the M.E.C.D. grant No. AP2000-1953.

[1] M. Smy, talk at Neutrino 2002, http://neutrino2002.ph.tum.de/ and hep-ex/0202020; Super-Kamiokande Collaboration, S. Fukuda *et al.*, Phys. Lett. B **539**, 179 (2002); Y. Fukuda *et al.*, Phys. Rev. Lett. **81**, 1158 (1998); **81**, 4279(E) (1998); **82**, 1810 (1999); **82**, 2430 (1999); Y. Suzuki, Nucl. Phys. B (Proc. Suppl.) **77**, 35 (1999); S. Fukuda *et al.*, hep-ex/0103032.

[2] B.T. Cleveland *et al.*, Astrophys. J. **496**, 505 (1998); R. Davis, Prog. Part. Nucl. Phys. **32**, 13 (1994).

[3] SAGE Collaboration, D.N. Abdurashitov *et al.*, Phys. Rev. C **60**, 055801 (1999); Zh. Eksp. Teor. Fiz. **122**, 211 (2002) [J. Exp. Theor. Phys. **95**, 181 (2002)].

[4] GALLEX Collaboration, W. Hampel *et al.*, Phys. Lett. B **447**, 127 (1999); GNO Collaboration, M. Altmann *et al.*, *ibid.* **490**, 16 (2000); GNO Collaboration, C. Cattadori, Nucl. Phys. B (Proc. Suppl.) **110**, 311 (2002); T. Kirsten, talk at Neutrino 2002, http://neutrino2002.ph.tum.de/.

[5] SNO Collaboration, Q.R. Ahmad *et al.*, Phys. Rev. Lett. **87**, 071301 (2001).

[6] SNO Collaboration, Q.R. Ahmad *et al.*, Phys. Rev. Lett. **89**, 011301 (2002).

[7] SNO Collaboration, Q.R. Ahmad *et al.*, Phys. Rev. Lett. **89**, 011302 (2002).

[8] O.G. Miranda *et al.*, Nucl. Phys. **B595**, 360 (2001); Phys. Lett. B **521**, 299 (2001), and references therein.

[9] J. Barranco, O.G. Miranda, T.I. Rashba, V.B. Semikoz, and J.W. Valle, Phys. Rev. D **66**, 093009 (2002).
[10] M. Guzzo *et al.*, Nucl. Phys. **B629**, 479 (2002), and references therein.
[11] Kamiokande Collaboration, Y. Fukuda *et al.*, Phys. Lett. B **335**, 237 (1994); IMB Collaboration, R. Becker-Szendy *et al.*, Nucl. Phys. B (Proc. Suppl.) **38**, 331 (1995); Soudan Collaboration, W.W.M. Allison *et al.*, Phys. Lett. B **449**, 137 (1999).
[12] MACRO Collaboration, M. Ambrosio *et al.*, Phys. Lett. B **434**, 451 (1998); M. Spurio *et al.*, hep-ex/0101019; B. Barish, talk given at *Neutrino 2000*, Sudbury, Canada, http://nu2000.sno.laurentian.ca.
[13] M. Shiozawa, talk at Neutrino 2002, http://neutrino2002.ph.tum.de/; Super-Kamiokande Collaboration, Y. Fukuda *et al.*, Phys. Rev. Lett. **81**, 1562 (1998).
[14] A. Surdo, Talk given at *TAUP 2001*, 2001, Gran Sasso, Italy, http://www.lngs.infn.it/.
[15] CHOOZ Collaboration, M. Apollonio *et al.*, Phys. Lett. B **466**, 415 (1999); Palo Verde Collaboration, F. Boehm *et al.*, Phys. Rev. D **64**, 112001 (2001).
[16] J.T. Peltoniemi, D. Tommasini, and J.W.F. Valle, Phys. Lett. B **298**, 383 (1993).
[17] J.T. Peltoniemi and J.W.F. Valle, Nucl. Phys. **B406**, 409 (1993).
[18] D.O. Caldwell and R.N. Mohapatra, Phys. Rev. D **48**, 3259 (1993).
[19] A. Ioannisian and J.W.F. Valle, Phys. Rev. D **63**, 073002 (2001); R.N. Mohapatra, A. Perez-Lorenzana, and C.A. de S Pires, Phys. Lett. B **491**, 14 (2000).
[20] M. Hirsch and J.W.F. Valle, Phys. Lett. B **495**, 121 (2000).
[21] Web-page of C. Giunti and M. Laveder, http://www.to.infn.it/~giunti/neutrino/
[22] LSND Collaboration, C. Athanassopoulos *et al.*, Phys. Rev. Lett. **77**, 3082 (1996); **81**, 1774 (1998); A. Aguilar *et al.*, Phys. Rev. D **64**, 112007 (2001).
[23] M. Maltoni, T. Schwetz, and J.W.F. Valle, Phys. Rev. D **65**, 093004 (2002).
[24] M. Maltoni, T. Schwetz, M.A. Tortola, and J.W. Valle, Nucl. Phys. **B643**, 321 (2002).
[25] J.N. Bahcall, M.C. Gonzalez-Garcia, and C. Pena-Garay, J. High Energy Phys. **07**, 054 (2002).
[26] A. Bandyopadhyay, S. Choubey, S. Goswami, and D.P. Roy, Phys. Lett. B **540**, 14 (2002).
[27] V. Barger, D. Marfatia, K. Whisnant, and B.P. Wood, Phys. Lett. B **537**, 179 (2002).
[28] P. Aliani *et al.*, Phys. Rev. D (to be published), hep-ph/0205053.
[29] P.C. de Holanda and A.Yu. Smirnov, Phys. Rev. D **66**, 113005 (2002).
[30] P. Creminelli *et al.*, J. High Energy Phys. **05**, 052 (2001).
[31] G.L. Fogli, E. Lisi, A. Marrone, D. Montanino, and A. Palazzo, Phys. Rev. D **66**, 053010 (2002).
[32] J.N. Bahcall, M.C. Gonzalez-Garcia, and C. Pena-Garay, Phys. Rev. C **66**, 035802 (2002).
[33] M.C. Gonzalez-Garcia, M. Maltoni, and C. Pena-Garay, Phys. Rev. D **64**, 093001 (2001).
[34] C. Giunti, M.C. Gonzalez-Garcia, and C. Pena-Garay, Phys. Rev. D **62**, 013005 (2000).
[35] J.N. Bahcall, M.H. Pinsonneault, and S. Basu, Astrophys. J. **555**, 990 (2001); see also Bahcall's page http://www.sns.ias.edu/~jnb/ and references therein.
[36] A.R. Junghans *et al.*, Phys. Rev. Lett. **88**, 041101 (2002).
[37] M.C. Gonzalez-Garcia, P.C. de Holanda, C. Pena-Garay, and J.W. Valle, Nucl. Phys. **B573**, 3 (2000).
[38] M.C. Gonzalez-Garcia, M. Maltoni, C. Pena-Garay, and J.W.F. Valle, Phys. Rev. D **63**, 033005 (2001); N. Fornengo, M.C. Gonzalez-Garcia, and J.W.F. Valle, Nucl. Phys. **B580**, 58 (2000); M.C. Gonzalez-Garcia, H. Nunokawa, O.L.G. Peres, and J.W.F. Valle, *ibid.* **B543**, 3 (1993).
[39] J.N. Bahcall, M.C. Gonzalez-Garcia, and C. Pena-Garay, J. High Energy Phys. **04**, 007 (2002).
[40] K. Kubodera's web-page http://nuc003.psc.sc.edu/~kubodera/.
[41] A.M. Dziewonski and D.L. Anderson, Phys. Earth Planet. Inter. **25**, 297 (1981).
[42] P.C. de Holanda, C. Pena-Garay, M.C. Gonzalez-Garcia, and J.W.F. Valle, Phys. Rev. D **60**, 093010 (1999); G.L. Fogli *et al.*, *ibid.* **62**, 113004 (2000); E. Lisi *et al.*, *ibid.* **63**, 093002 (2001); E. Lisi and D. Montanino, *ibid.* **56**, 1792 (1997).
[43] J.N. Bahcall, P.I. Krastev, and A.Y. Smirnov, Phys. Rev. D **60**, 093001 (1999).
[44] A. Strumia *et al.*, Phys. Lett. B **541**, 327 (2002).
[45] M.C. Gonzalez-Garcia and M. Maltoni, hep-ph/0202218.
[46] M. Maltoni, T. Schwetz, and J.W.F. Valle, Phys. Lett. B **518**, 252 (2001).
[47] W.W.M. Allison *et al.*, Phys. Lett. B **449**, 137 (1999); M. Goodman, talk at Neutrino 2002, http://neutrino2002.ph.tum.de/
[48] M.C. Gonzalez-Garcia, H. Nunokawa, O.L. Peres, T. Stanev, and J.W. Valle, Phys. Rev. D **58**, 033004 (1998).
[49] G. Barr, T.K. Gaisser, and T. Stanev, Phys. Rev. D **39**, 3532 (1989); T.K. Gaisser, T. Stanev, and G. Barr, *ibid.* **38**, 85 (1988); T.K. Gaisser and T. Stanev, *ibid.* **57**, 1977 (1998).
[50] G.L. Fogli, E. Lisi, and A. Marrone, Phys. Rev. D **64**, 093005 (2001).
[51] E.K. Akhmedov and J. Pulido, hep-ph/0209192.
[52] KamLAND Collaboration, A. Piepke, Nucl. Phys. B (Proc. Suppl.) **91**, 99 (2001); http://kamland.lbl.gov/KamLAND